Science of the Total Environment 779 (2021) 146570

Contents lists available at ScienceDirect

Science of the Total Environment

journal homepage: www.elsevier.com/locate/scitotenv

Anthropogenic CO_2 and ocean acidification in Argentine Basin Water Masses over almost five decades of observations

Marcos Fontela [a,b,*], Antón Velo [b], Miguel Gilcoto [b], Fiz F. Pérez [b]

[a] Center of Marine Sciences (CCMAR), Universidade do Algarve, 8005-139 Faro, Portugal
[b] Instituto de Investigaciones Marinas, IIM-CSIC, 36208 Vigo, Spain

HIGHLIGHTS

- In the Argentine Basin there is an increase in anthropogenic carbon at all depths.
- Acidification by carbon uptake is being enhanced by natural processes.
- The loss of carbonate affects upper and intermediate water masses: SACW, SAMW, AAIW
- The imminent carbonate undersaturation in AAIW is virtually unavoidable.

GRAPHICAL ABSTRACT

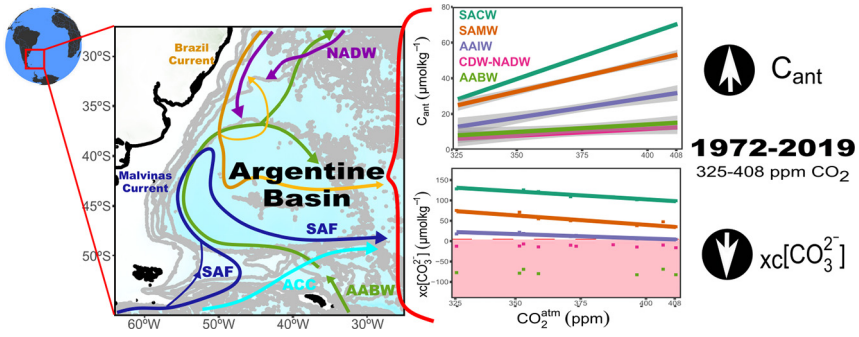

ARTICLE INFO

Article history:
Received 12 November 2020
Received in revised form 9 March 2021
Accepted 14 March 2021
Available online 19 March 2021

Guest Editor: Jesús Forja

Keywords:
Ocean acidification
Anthropogenic carbon
Carbonate
Deoxygenation
Argentine basin
Western South Atlantic

ABSTRACT

The chemical conditions of the Argentine Basin (western South Atlantic Ocean) water masses are evaluated with measurements from eleven hydrographic cruises to detect and quantify anthropogenic and natural stressors in the ocean carbon system. The database covers almost half-century (1972–2019), a time-span where the mean annual atmospheric carbon dioxide concentration (CO_2^{atm}) increased from 325 to 408 ppm of volume (ppm). This increase of atmospheric CO_2 (83 ppm, the 64% of the total anthropogenic signal in the atmosphere) leads to an increase in anthropogenic carbon (C_{ant}) across all the water column and the consequent ocean acidification: a decrease in excess carbonate that is unequivocal in the upper (South Atlantic Central Water, SACW) and intermediate water masses (Sub Antarctic Mode Water, SAMW and Antarctic Intermediate Water, AAIW). For each additional ppm in CO_2^{atm} the water masses SACW, SAMW and AAIW lose excess carbonate at a rate of 0.39 ± 0.04, 0.47 ± 0.05 and 0.23 ± 0.03 μmol·kg^{-1}·ppm^{-1} respectively. Modal and intermediate water masses in the Argentine Basin are very sensitive to carbon increases due low buffering capacity. The large rate of AAIW acidification is the synergic effect of carbon uptake combined with deoxygenation and increased remineralization of organic matter. If CO_2 emissions follows the path of business-as-usual emissions (SSP 5.85), SACW would become undersaturated with respect to aragonite at the end of the century. The undersaturation in AAIW is virtually unavoidable.

© 2021 The Author(s). Published by Elsevier B.V. This is an open access article under the CC BY-NC-ND license (http://creativecommons.org/licenses/by-nc-nd/4.0/).

1. Introduction

The unabated increase in atmospheric carbon dioxide (CO_2^{atm}) concentration due anthropogenic emissions is the main driver of the current climate change (Pörtner et al., 2019). The uptake of an important fraction (~30%) of the anthropogenic carbon dioxide by the ocean (C_{ant}), mitigates global warming reducing the rate of increase in CO_2^{atm}

* Corresponding author at: Center of Marine Sciences (CCMAR), Universidade do Algarve, 8005-139 Faro, Portugal.
E-mail addresses: mmfontela@ualg.pt (M. Fontela), avelo@iim.csic.es (A. Velo), mgilcoto@iim.csic.es (M. Gilcoto), fiz.perez@iim.csic.es (F.F. Pérez).

https://doi.org/10.1016/j.scitotenv.2021.146570
0048-9697/© 2021 The Author(s). Published by Elsevier B.V. This is an open access article under the CC BY-NC-ND license (http://creativecommons.org/licenses/by-nc-nd/4.0/).

(Sabine et al., 2004). This C_{ant} uptake has a negative counterpart for the ocean: a change in their chemical conditions that is commonly referred to as ocean acidification (Caldeira and Wickett, 2003; Raven et al., 2005). Like climate change, ocean acidification is a global process with spatial heterogeneities: the Atlantic Ocean, due to its chemical properties and meridional circulation (Perez et al., 2018), is the ocean with the largest C_{ant} storage (Khatiwala et al., 2013). While the North Atlantic has received much more attention (Fröb et al., 2018; Pérez et al., 2013; Pérez et al., 2010), the South Atlantic rate of C_{ant} increase has been argue to be even larger than in the North Atlantic (Wanninkhof et al., 2010). The convey of C_{ant} loaded mode and intermediate waters through the upper cell of the meridional overturning circulation in the Southern Hemisphere (Pardo et al., 2014) results in large storage rates within the latitude band 50°-30°S (Mikaloff Fletcher et al., 2006). In the South Atlantic, where an anomalously high accumulation of C_{ant} have been reported for the period 1994–2007 (Gruber et al., 2019), the western basins (Argentine Basin, Brazil Basin) are the main regions for the sink of C_{ant} (Ríos et al., 2012).

In the Argentine Basin, a region with high primary production (Behrenfeld and Falkowski, 1997) and a strong CO_2^{atm} sink (Rödenbeck et al., 2015), the subduction of modal and intermediate water masses of subantarctic origin below subtropical water masses isolates them from atmospheric influence (Jullion et al., 2010). In analogy with North Atlantic deep water formation regions that are hotspots for tracers to be conveyed through the interior ocean (Perez et al., 2018) and long-time sequestered (Fontela et al., 2019), the influence of this subduction in the chemical status of the water masses require a close-up evaluation with the newest data available.

The Argentine Basin is characterized for the confluence of Antarctic water masses and water masses coming from the north (Stramma and England, 1999; Valla et al., 2018). The upper layer circulation is conditioned by the Malvinas Current, the northernmost branch of the Antarctic Circumpolar Current (Subanctartic Front, SAF) in their northward cyclonic loop over the Argentine Basin (Fig. 1). The cold and fresh Malvinas Current, that was originated in the Drake Passage, encounters the southward flowing western boundary current of the South Atlantic subtropical gyre, the Brazil Current (Jullion et al., 2010). The highly dynamic region of transition between these two currents is the Brazil–Malvinas Confluence (BMC, Fig. 1) (Artana et al., 2018). The intermediate circulation is characterized by the northward circulation of Antarctic Intermediate Water (AAIW). Deep circulation is marked by the collide between Circumpolar Deep Water (CDW) in northward direction and North Atlantic Deep Water (NADW) flowing southward within the deep western boundary current (Mémery et al., 2000). In the abyssal layer Antarctic Bottom Water (AABW), the coldest and densest water mass produced in the Southern Ocean, spreads northward constrained by bottom topography (Talley et al., 2011).

Argentine Basin water masses has gain C_{ant} and suffer acidification (Orselli et al., 2018; Salt et al., 2015) from the surface to the bottom (Ríos et al., 2015; Ríos et al., 2012). AAIW and CDW are water masses very sensitive to changes in carbonate due C_{ant} uptake (González-Dávila et al., 2011). Furthermore, the content of dissolved oxygen (O_2) is declining in the South Atlantic during the past five decades of observations (Schmidtko et al., 2017). In this century, not only the formation of AABW has been reduced (De Lavergne et al., 2014), but also it has warmed (Johnson et al., 2020; Meinen et al., 2020; Zenk and Morozov, 2007), freshened (Anilkumar et al., 2015; Jullion et al., 2013; Menezes et al., 2017; Rintoul, 2007; Swift and Orsi, 2012) and acidified (Ríos et al., 2015).

All these characteristics, in combination with their geographical location close to the Southern Ocean, makes this basin relevant for the carbon cycle at global scale. In this study, almost five-decades of ocean acidification trends across the whole water column of the Argentine Basin are evaluated with the most updated databases based on in situ measurements of carbon-system variables.

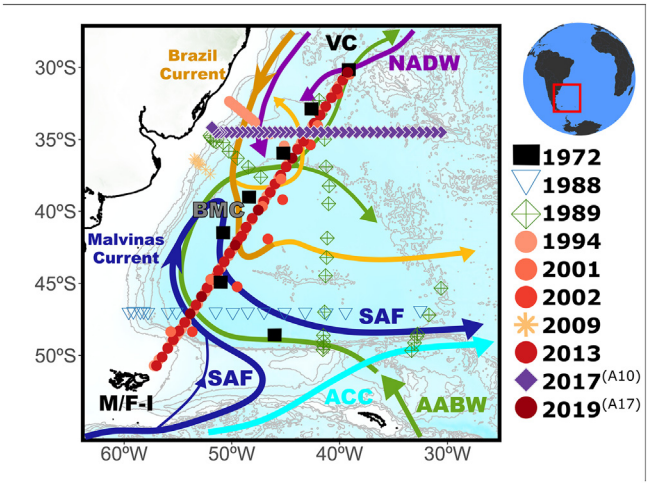

Fig. 1. Map of the Argentine basin in the Southwest Atlantic Ocean. The location of the stations used in this study and the year are represented according with the legend. Note that the years 1994, 2001, 2002, 2013 and 2019 are repetitions of the same section. The Vema Channel (VC) and the Malvinas/Falkland Islands (M/F-I) are the northern and southern limits respectively of the measurements used in this study. The westernmost limit is the Patagonian shelf and the easternmost limit is the 30°W longitude. The schematic diagram of the large-scale circulation is adapted from Mémery et al., (2000); Stramma and England, (1999); Talley et al., (2011) and Valla et al., (2018). The track of cruises represented in Figs. 2 and 3 across the GO-SHIP A17 (A10) section is represented with red circles (purple diamonds). Acronyms: Subanctarctic Front (SAF), Antarctic Circumpolar Current (ACC), Brazil-Malvinas Confluence (BMC), North Atlantic Deep Water (NADW), Antarctic Bottom Water (AABW).

2. Data and methods

2.1. Database assembling

The Argentine Basin is defined by the oceanic realm comprised between latitudes 51°–30° S and longitudes 60°–30° W. In that region, data mining of high-quality oceanographic chemical tracers: nutrients (nitrate –NO_3–, phosphate –PO_4–, silicate –SiO_4–) and carbon system variables (pH, dissolved inorganic carbon –DIC-, total alkalinity –TA–) were gathered to evaluate the evolution of the chemical conditions (C_{ant}, excess carbonate –$_{xc}[CO_3^{2-}]$–) in the Argentine Basin. Only cruises with measurements for at least two carbon variables (pH/TA, TA/DIC, DIC/pH, Supp. Info Table S1) were selected. The assembled database comprised a total of eight cruises presents in GLODAPv2 (Olsen et al., 2016, 2020) and three cruises in CLIVAR, Carbon Hydrographic Data Office (http://cchdo.ucsd.edu/). These datasets are subject to quality control procedures (Key et al., 2010, 2015; Velo et al., 2010) and each water sample is flagged properly. The complete list of cruises (eleven) with their correspondent *Expocode* is available in Supp. Info Table 1. The combined dataset has a time span of 47 years (1972–2019). The last two cruises, 2017 and 2019, are in GLODAP since the update of 2019 (Olsen et al., 2019) and 2020 (Olsen et al., 2020), respectively.

Table 1
Water mass vertical distribution into layers delimited by potential density ($\sigma_{refpressure}$) isopycnals. Water mass names, acronyms, and upper and lower limits of potential density.

Water masses	Acronym	Upper limit ($kg \cdot m^{-3}$)	Lower limit ($kg \cdot m^{-3}$)
South Atlantic Central Water	SACW	>100 m	$\sigma_0 = 26.5$
Sub Antarctic Mode Water	SAMW	$\sigma_0 = 26.50$	$\sigma_0 = 27.10$
Antarctic Intermediate Water	AAIW	$\sigma_0 = 27.10$	$\sigma_0 = 27.40$
Circumpolar Deep Water – North Atlantic Deep Water	CDW-NADW	$\sigma_0 = 27.40$	$\sigma_4 = 45.90$
Antarctic Bottom Water	AABW	$\sigma_4 = 45.90$	Seafloor

To the best of our knowledge, high-quality carbon measurements (pH and TA) for the GO-SHIP A17 section in the year 2019 (April–May, R/V BIO Hespérides), included here, has not been used up to date in any other study.

2.2. Layer separation

The main water masses found in the Argentine Basin have specific properties in temperature, salinity, inorganic nutrients and ventilation tracers (CFCs) that allows their recognition (Mémery et al., 2000). The vertical water mass distribution along the whole water column is delimited in five layers by potential density isopycnals (Table 1, Fig. 2). Previous studies in the zone have used similar water mass characterization (Ríos et al., 2015; Ríos et al., 2012; Salt et al., 2015). As the current analysis is focused exclusively in the Argentine Basin, and not in the southwestern Atlantic (Ríos et al., 2012; Salt et al., 2015) or the complete Atlantic Ocean (Ríos et al., 2015), some adjustments has been made to the layer separation: CDW and NADW share the same isopycnals and they are not divided in upper and lower cores.

The no separation between CDW and NADW is based in (i) the fact that they collide with each other at the same densities (Mémery et al., 2000); (ii) that south of Vema Channel (our northern limit) the NADW progresses as a relatively saline tongue between CDW at depths 2000–4000 m (Álvarez et al., 2014), and therefore, a careful analysis of the diapycnal mixing processes would be required to disentangle water masses in this layer, and last; (iii) that similar water mass characterization was used in previous studies (Ríos et al., 2012).

The surface layer (<100 m) is not included in the calculation of the mean annual layer concentration to avoid seasonal effects. Seasonality in the surface most layer cannot be evaluated with the assembled Argentine Basin database, since it does not include carbon measurements between the months May to October (Supp. Info Fig. S1).

2.3. Carbon system calculations

Carbon system calculations follows the recommendations by Dickson et al. (2007) and were done with the CO_2 dissociation constants of Lueker et al. (2000), the constant for the sulphate dissociation of Dickson (1990) and the constant for fluoride association of Pérez and Fraga (1987). For the concentration of total boron it was used the Uppström (1974) formulation. Computations were done in the R language with the public software package *Seacarb* (Gattuso et al., 2020).

Anthropogenic carbon (C_{ant}) was estimated with the biogeochemical back-calculation ϕCT° method (Pérez et al., 2008; Vázquez-Rodríguez et al., 2009). It is a process-oriented method that uses the subsurface layer as reference for water mass formation conditions avoiding the seasonal variability of the upper layers (Vázquez-Rodríguez et al., 2012). Furthermore, the method does not set an arbitrary zero-C_{ant} reference which introduce bias in deep-water C_{ant} estimates (Lo Monaco et al., 2005). The ϕCT° method has been validated for the South Atlantic (Vázquez-Rodríguez et al., 2009) and has an overall uncertainty of ±5.2 μmol kg^{-1}. The difference between DIC and C_{ant} is the natural fraction of dissolved inorganic carbon (DIC_{nat} = DIC - C_{ant}).

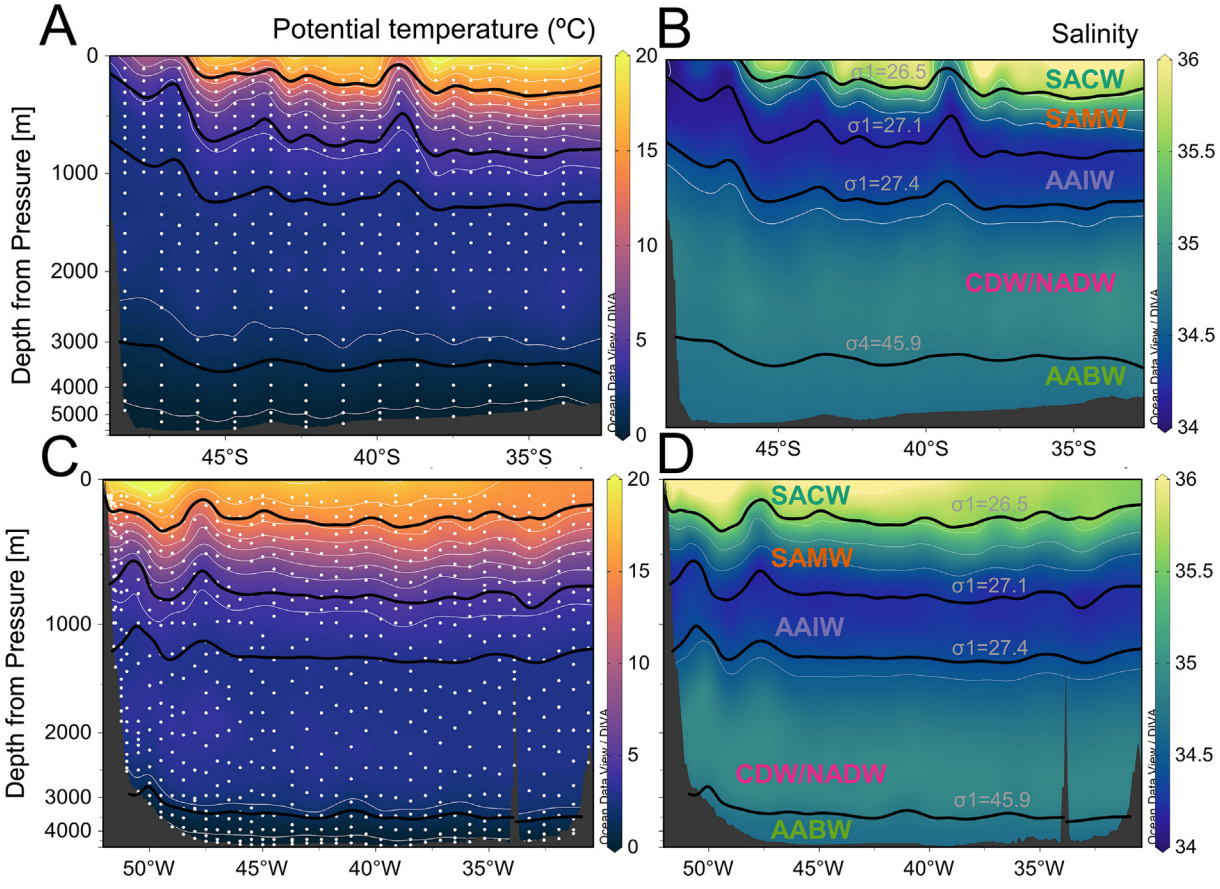

Fig. 2. Vertical distribution of (A, C) potential temperature (°C) and (B, D) salinity for a latitudinal (A, B) and a longitudinal (C, D) section across the Argentine Basin. Latitudinal transect (from 50°S to 30°S, upper figures) is from the A17 section south of Vema Channel at the year 2019. Longitudinal transect (from 52°W to 30°W at the latitude band 35°S) is from A10 section at the year 2017. The plot is the vertical distribution (m) between surface and bottom (maximum depth around 6000 m at 46°S 53°W for the latitudinal section, and 4500 at 35°S 45°W for the longitudinal section). The water masses are separated by black lines of potential density according to the layer separation. White dots (A, C) represent samples. Note that the depth-scale is not linear. Sections were generated using Ocean Data View (Schlitzer, 2020).

The ratio between the ion product of the concentrations of calcium and carbonate and the aragonite solubility product (K_{Arg}) at in situ conditions of temperature, salinity, and pressure (Feely et al., 1984) is the in situ degree of aragonite saturation (Ω_{Arg}) (Eq. (1)):

$$\Omega_{Arg} = \frac{\left[Ca^{2+}\right]\left[CO_3^{2-}\right]_{is}}{K_{Arg}} \quad (1)$$

when $\Omega_{Arg} > 1$ ($\Omega_{Arg} < 1$), seawater is supersaturated (undersaturated) with respect to aragonite. The $[CO_3^{2-}]$ at saturation ($\Omega_{Arg} = 1$) is therefore (Eq. (2)):

$$\left[CO_3^{2-}\right]_{sat(\Omega_{Arg}=1)} = \frac{K_{Arg}}{\left[Ca^{2+}\right]} \quad (2)$$

the ratio between the stoichiometric solubility product (K_{Arg}) and the concentration of the conservative ion calcium ($[Ca^{2+}]$), that is dependent of salinity (Dickson et al., 2007; Millero et al., 2008). Both K_{Arg} and $[Ca^{2+}]$ were calculated with the *seacarb* package (Gattuso et al., 2020). The difference between $[CO_3^{2-}]_{is}$ and the $[CO_3^{2-}]$ at aragonite saturation ($[CO_3^{2-}]_{sat(\Omega Arg=1)}$), is the excess of carbonate over aragonite saturation ($_{xc}[CO_3^{2-}]$) (Orr et al., 2005; Perez et al., 2018). The use of $_{xc}[CO_3^{2-}]$ as a measure of the real concentration available for marine calcifiers has been used before as a quantitative measurement of the chemical conditions that marine calcifiers are exposed to (Fontela et al., 2020).

2.4. Statistical analysis

Mean annual water mass concentration for selected tracers grouped by year of the cruise and layer is compared against the main driver of climate change: the concentration of CO_2^{atm} (Stocker et al., 2013) in parts per million of volume (ppm). The robust fit to estimate tracer evolution (Figs. 4–5) is calculated with the function *rlm* of R package *MASS* (Venables and Ripley, 2002). The linear fit is done by iterated reweighted least squares, where the weights are the inverse of the standard deviation for all the available measurements for each year and layer. Note that with that weighting, we are using a cautionary approach because errors are larger than the computational uncertainties of the carbon system. Statistical results and rates of change with respect CO_2^{atm} concentration (in ppm) for the main climate change stressors are in Table 2 and Supp.Info Table S2. The rate of anthropogenic disturbance of chemical properties versus time is also available in Supp. Info Table S3. The number of samples by year and layer is available in Supp. Info Fig. S2.

2.5. Data availability

All the data used in this study come from the open access databases: GLODAPv2 (https://www.glodap.info/) and CLIVAR, Carbon Hydrographic Data Office (CCHDO, http://cchdo.ucsd.edu/).

The mean annual concentration of atmospheric CO_2 (in parts per million of volume, ppm) for the year of the cruise was taken from the ESRL's Global Monitoring Laboratory of the National Oceanic and Atmospheric Administration (NOAA) located in the South Pole (SPO) observatory (https://www.esrl.noaa.gov/gmd/obop/spo/) [Dlugokencky and Tans, (2020); last time accessed: 17/04/2020]. The CO_2 growth rate registered in the SPO is representative for the Southern Hemisphere (Ciais et al., 2019). The monthly concentration of atmospheric CO_2 at SPO is available since summer 1975. As the oldest data in our Argentine Basin database is from 1972, the mean annual concentration of atmospheric CO_2 for the year 1972 was estimated as the mean annual concentration of atmospheric CO_2 in Mauna Loa (available since 1959) corrected by the mean difference between annual values of Mauna Loa and SPO for the complete time series.

R code files to reproduce the Argentine Basin database, to analyse the data and to generate the results and the trend figures that support the findings of this study are available in the supplementary information and in the Github repository: https://github.com/mfontela/ArgentineBasin (Bengtsson, 2018; Dragulescu and Arendt, 2020; Fontela, 2021; Pante and Simon-Bouhet, 2013; Ren, 2016; Wickham et al., 2019).

3. Results

The vertical distribution of potential temperature and salinity across the Argentine Basin is shown in Fig. 2. The latitudinal section (50°-30° S, Fig. 2 A-B) is part of the GO-SHIP section A17 of 2019 (Expocode: 29HE20190406, Fig. 1). The longitudinal section (Fig. 2 C–D) is part of the GO-SHIP section A10 of 2017 (Expocode: 06M220170104, Fig. 1).

In temperature (salinity), there is latitudinal variability (Fig. 2A-B) in upper and intermediate layers with colder (fresher) waters in the southern region. In the surface, the gradient of thermohaline properties changes from cold, fresh waters in the southernmost latitudes towards warm (>20 °C) and salty (>36) waters towards 35°S. The eddies (44°S and 40°S, Fig. 2 A–B) are produced by the BMC while the SAF supposes a steep change in salinity towards fresher waters around 45°S. The subduction of upper and intermediate water masses under the upper-ocean water masses of the subtropical gyre is clearly visible in the latitudinal sections (Fig. 2 A-B) and their properties arrive until the northward limit of the basin (longitudinal sections, Fig. 2C–D).

Subantarctic Mode Water (SAMW) density band outcrops at the south of the SAF (~45°S), subducting modal water in equatorial direction just below poleward moving central waters (McCartney, 1982; McNeil et al., 2007). Alike, the upward tilt of the 27.1 $kg \cdot m^{-3}$ isopycnal, the upper limit of AAIW, points that the outcrop of this intermediate water mass is south of the Argentine Basin (Fig. 2A), in the Drake Passage (Evans et al., 2017). Once stabilized after subduction, the limit between AAIW and deeper waters is located around 1200 m north of SAF. There is a salinity minimum in the first 500 m depth at latitudes south of SAF that deepens northward and follow the $27.1 < \sigma_0 < 27.4$ potential density line (700–1200 m depth) moving with the AAIW in equatorward direction. The AAIW is identified all along the Argentine Basin as a band of lower salinity than its surroundings. Below AAIW and to ~3200 m depth, the largest volume in the Argentine basin is occupied by the density band where CDW and NADW collide with each other. The amount of CDW flowing from the Antarctic Circumpolar

Table 2
Observed trends in Argentine Basin water masses. Water mass acronyms: South Atlantic Central Water (SACW), Subantarctic Mode Water (SAMW), Antarctic Intermediate Water (AAIW), Circumpolar Deep Water and North Atlantic Deep Water (CDW-NADW) and Antarctic Bottom Water (AABW). Only robust fit trends with a statistical *p*-value <0.005 have been included. $pH_{is}T$ is in total scale at in situ (subscript "*is*") conditions.

Water masses	C_{ant} (μmol kg^{-1} ppm^{-1})	$_{xc}[CO_3^{2-}]$ (μmol kg^{-1} ppm^{-1})	pHisT (x10^3 pH units ppm^{-1})	DIC_{nat} (μmol kg^{-1} ppm^{-1})
SACW	0.51 ± 0.02	−0.39 ± 0.04	−1.06 ± 0.05	0.16 ± 0.05
SAMW	0.35 ± 0.03	−0.47 ± 0.06	−1.50 ± 0.09	0.28 ± 0.04
AAIW	0.23 ± 0.05	−0.23 ± 0.03	−1.09 ± 0.13	0.15 ± 0.07
CDW-NADW	0.09 ± 0.03			
AABW	0.11 ± 0.04			0.03 ± 0.01

Current (ACC, Fig. 1) occupies more volume in the basin than NADW, but the relevance of NADW increases towards the northward limit (Álvarez et al., 2014). This can also be seen in the deep salinity maximum near the Vema Channel that is associated with NADW coming from the north (Fig. 2B at latitudes <35°S and Fig. 2D at 1500-3000 m depth). There are potential temperatures below 0 °C in the deepest layer of AABW. In AABW there is a northward increase in temperature (salinity) due progressive mixing with the warmer (saltier) NADW above it.

The vertical distribution of $_{xc}[CO_3^{2-}]$ and C_{ant} across the Argentine Basin is shown in Fig. 3. Vertical distribution shows high C_{ant} values near the surface (~70–80 μmol·kg^{-1}), a subsequent decrease with depth, and a further increase in the deepest layers. The gradient of decrease is particularly strong in the intermediate layers, from surface to 1000 m depth. Below AAIW, concentrations remain almost constant (<10 μmol·kg^{-1}) until bottom waters that are above 10 μmol·kg^{-1}. C_{ant} is detected across all depth levels and the C_{ant} penetration follows the subducted isopycnals. The latitudinal section show that upper layers increase their C_{ant} content in equatorward direction, in agreement with the current view that subtropical waters are important C_{ant} uptake zones (Gruber et al., 2019). The longitudinal section depicts very well the progression of AABW with C_{ant} values higher than 10 μmol·kg^{-1} below the NADW intrusion that progress through the Vema Channel and the western boundary current (Fig. 3C–D).

The $_{xc}[CO_3^{2-}]$ values decrease with depth, from supersaturated ($_{xc}[CO_3^{2-}] > 0$) surface waters with more than 100 μmol kg^{-1} of $_{xc}[CO_3^{2-}]$, towards abyssal values below −100 μmol kg^{-1} under saturation ($_{xc}[CO_3^{2-}] < 0$). At mid-depths there are lower $_{xc}[CO_3^{2-}]$ values in the southern end, creating a gradual southward upward tilt of the isolines. The lowest $_{xc}[CO_3^{2-}]$ is found in the AABW layer at abyssal depths (>6000 m, −130 μmol·kg^{-1}, Supp. Info. Fig. S3). The longitudinal sections (Fig. 2 C–D) show no west-east gradients, with the exception of a pocket of undersaturated water around 2000 m depth close to the Patagonian shelf slope (Fig. 2 D) that is related with the intrusion of NADW from the Deep Western Boundary Current (Rhein et al., 2015). South of SAF, the aragonite saturation horizon (ASH) shoals until 700 m. North of the SAF, the ASH takes place at ~1000 m, in agreement with the distribution of ASH in the South Atlantic (Jiang et al., 2015). The upward tilt of the 0 μmol·kg^{-1} isoline that occurs south of the SAF is due downwelling of recently formed water masses with low $_{xc}[CO_3^{2-}]$ (AAIW, SAMW).

The temporal evolution of mean C_{ant} averages in each of the five layers for the period between 325 and 408 ppm (1972–2019) is represented in Fig. 4. The gradient of concentrations between surface and bottom waters has almost tripled. In 1972 there was a difference of ~20 μmol·kg^{-1} (less than 30 and 10 μmol·kg^{-1} in the upper and deeper layer, respectively) that is around ~55 μmol·kg^{-1} in 2019 (concentrations larger than 70 μmol·kg^{-1} in upper central waters and 15 μmol·kg^{-1} in the deeper layer). The uncertainties of the mean C_{ant} averages, expressed as standard deviation of the samples, are dependent not only of the number of samples by year and layer but also the geographical extent of the samples related with the cruise track.

The increase in C_{ant} exists across all depths and water masses. The trends decrease with depth: while SACW shows a rate of change of 0.51 ± 0.02 μmol·kg^{-1} ppm^{-1}, AAIW has a trend that is almost half of that (0.23 ± 0.05 μmol·kg^{-1} ppm^{-1}), with SAMW in between (0.35 ± 0.03 μmol·kg^{-1} ppm^{-1}). In the two deep layers, CDW-NADW

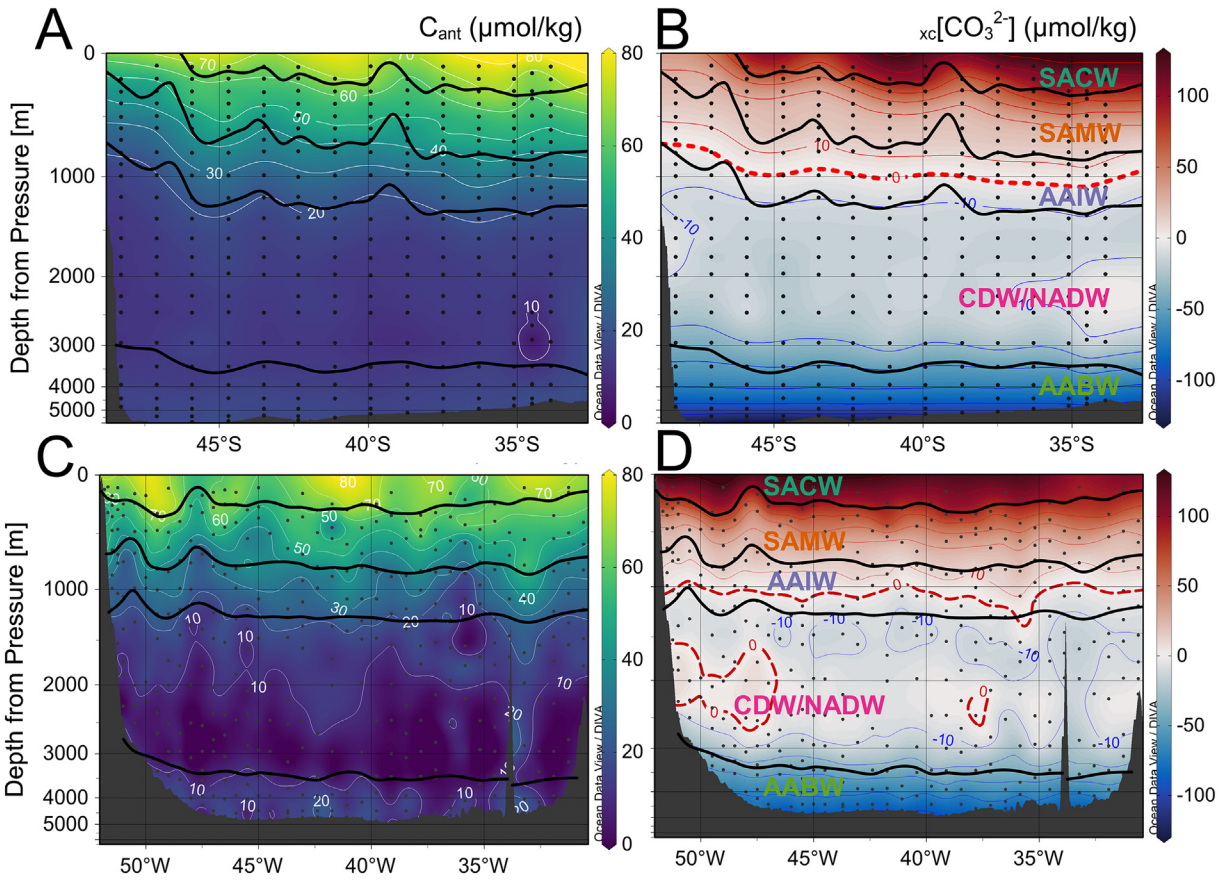

Fig. 3. Vertical distribution of (A, C) anthropogenic carbon (C_{ant}, μmol kg^{-1}) and (B, D) $_{xc}[CO_3^{2-}]$ (μmol kg^{-1}) for a latitudinal (A, B) and a longitudinal (C, D) section across the Argentine Basin. The red dash line (B, D) is the Aragonite Saturation Horizon (ASH, 0 μmol kg^{-1}). Latitudinal transect (from 50°S to 30°S, upper figures) is from the A17 section south of Vema Channel at the year 2019. Longitudinal transect (from 52°W to 30°W at the latitude band 35°S) is from A10 section at the year 2017. The plot is the vertical distribution (m) between surface and bottom (maximum depth around 6000 m at 46°S 53°W for the latitudinal section, and 4500 m at 35°S 45°W for the longitudinal section). The water masses are separated by black lines of potential density according to the layer separation (acronyms and density values are detailed in Table 1). Black dots represent samples. Note that the depth-scale is not linear. Sections were generated using Ocean Data View (Schlitzer, 2020).

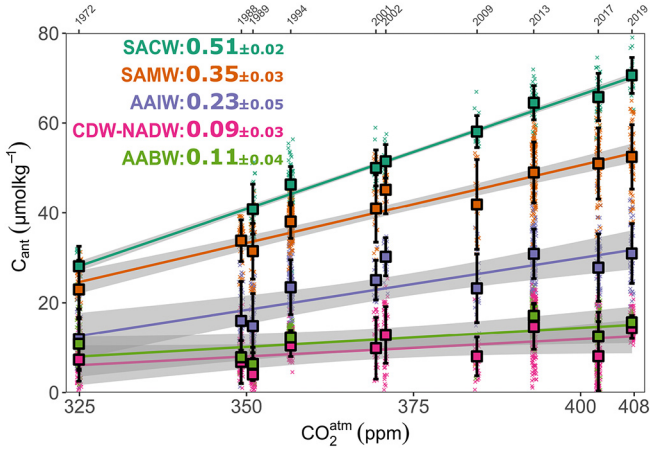

Fig. 4. Mean water mass anthropogenic carbon (C_{ant}, μmol kg^{-1}) versus atmospheric CO_2 concentration (ppm) in the Argentine Basin. SACW (cyan), SAMW (orange), AAIW (purple) CDW-NADW (pink) and AABW (light green). All the used data is represented with small size crosses. Mean annual concentration by layer is represented with filled squares with a black stroke. Vertical black lines around the annual mean properties are the uncertainties expressed with the standard deviation. Only robust fit trends (μmol·kg^{-1}·ppm^{-1}) with a statistical *p*-value <0.05 have been depicted (Table 2), and the observed trend is included as a text annotation following the same colour code. The year of the cruise is represented in the upper x-axis.

and AABW, the trends are similar. AABW shows an upward trend of 0.11 ± 0.04 μmol·kg^{-1} ppm^{-1} and slightly higher concentrations than CDW-NADW. Uncertainties in the trends increase with depth mainly due less number of samples.

The evolution of $_{xc}[CO_3^{2-}]$ with respect CO_2^{atm} is represented in Fig. 5. While the saturated water masses in the upper and intermediate layers shows decreasing trends, the trend does not exist in the already undersaturated water masses (CDW-NADW and AABW). The highest $_{xc}[CO_3^{2-}]$ decrease is not in the uppermost SACW (−0.39 ± 0.04 μmol·kg^{-1} ppm^{-1}) instead in the modal water, SAMW (−0.47 ± 0.06 μmol·kg^{-1} ppm^{-1}). The initial $_{xc}[CO_3^{2-}]$ was close to 20 μmol·kg^{-1} in AAIW and is now close to the limit of undersaturation (<0 $_{xc}[CO_3^{2-}]$ μmol·kg^{-1}).

Following with the cautionary approach when dealing with uncertainties, the mean $_{xc}[CO_3^{2-}]$ error that weight the linear model adjustment is 15.5 μmol·kg^{-1}. As example, the minimum error for $_{xc}[CO_3^{2-}]$ (6.2 μmol·kg^{-1} in the CDW-NADW layer, computed with 21 samples over the 2001 track of the A17 section) is still higher than when computed with the uncertainty propagation method (±3.7 μmol kg^{-1}, Orr et al., 2018).

4. Discussion

The results are supported by ocean carbon measurements spanning 47 years, a period that comprised a total increase in the CO_2^{atm} concentration of 83 ppm. The rate of CO_2^{atm} increase has been above the mean (>1.7 ppm/yr^{-1}) since the onset of the XXIst century (2.1 ppm/yr^{-1}, Dlugokencky and Tans, 2020). Changes in potential temperature, salinity and/or alkalinity can be discarded as stressors of climate change in Argentine Basin water masses since they do not show any trend at all (Supp. Info Fig. S3).

This study extends the time span of previous studies of southwestern Atlantic Ocean acidification by fourteen (Ríos et al., 2012), nine (Salt et al., 2015) and six years (Ríos et al., 2015). The formation and subduction of mode and intermediate water masses conveys C_{ant} through the interior Ocean (Sabine et al., 2004). The largest C_{ant} concentrations (>70 μmol·kg^{-1}) exists in the central water mass, SACW, in analogy with the North Atlantic Central Water in the northern hemisphere (Fontela et al., 2020). Water masses with recent ventilation and subduction have higher C_{ant} concentrations (Pérez et al., 2008; Ríos et al., 2010). The observed water masses trends for C_{ant} are essentially in agreement with previous evaluations in the South Atlantic. The C_{ant} uptake rate in SACW (0.51 ± 0.02 μmol·kg^{-1} ppm^{-1}) is lower than previously reported (SACW 0.63 ± 0.01 μmol·kg^{-1} ppm^{-1}, Ríos et al., 2012). The higher value in Ríos et al. (2012) is related with the fact that they included a larger subtropical area where the SACW is more dominant, and it is in the subtropical areas where water masses reach C_{ant} concentrations at saturation levels (Gruber et al., 2019). The C_{ant} increase rate in the modal water SAMW (0.35 ± 0.03 μmol·kg^{-1} ppm^{-1}, Table 2) and in AAIW (0.23 ± 0.05 μmol·kg^{-1} ppm^{-1}), when expressed against the time in years are 0.62 ± 0.03 μmol·kg^{-1} yr^{-1} and 0.42 ± 0.08 μmol·kg^{-1} yr^{-1} (Supp. Info Table S3). These values are 17% larger than 0.53 μmol·kg^{-1} yr^{-1} and 0.36 μmol·kg^{-1} yr^{-1} previously reported for SAMW and AAIW, respectively (Ríos et al., 2012; Salt et al., 2015). The synergic effect of two causes are the reason behind this increase. First, the geographical boundaries of this analysis are exclusively restricted to the Argentine Basin, with younger water masses than across the complete southwestern Atlantic (Ríos et al., 2012; Salt

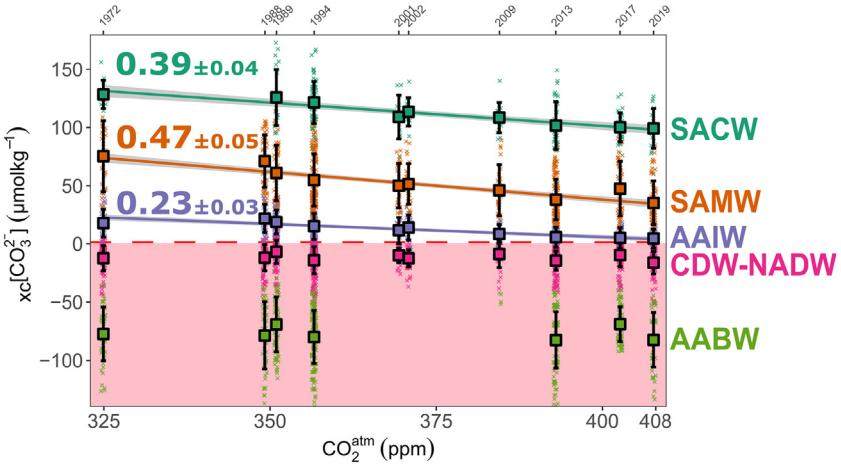

Fig. 5. Mean water mass $_{xc}[CO_3^{2-}]$ (μmol kg^{-1}) versus atmospheric CO_2 concentration (ppm) in the Argentine Basin. SACW (cyan), SAMW (orange), AAIW (purple) CDW-NADW (pink) and AABW (light green). All the used data is represented with small size crosses. Mean annual concentration by layer is represented with filled squares with a black stroke. Vertical black lines around the annual mean properties are the uncertainties expressed with the standard deviation. Only robust fit trends (μmol·kg^{-1}·ppm^{-1}) with a statistical p-value <0.05 have been depicted (Table 2), and the observed trend is included as a text annotation following the same colour code. The light red zone below the limit of 0 $_{xc}[CO_3^{2-}]$ represents undersaturated waters with respect to aragonite. The year of the cruise is represented in the upper x-axis.

et al., 2015;). Second; the larger time span of our study is associated with an increasing growth rate of CO_2^{atm} (Dlugokencky and Tans, 2020) and with the current trend of increase in CO_2 uptake in the area after 2000 (Landschützer et al., 2016; Rödenbeck et al., 2015). In contrast, the C_{ant} uptake trend reported in the AAIW layer (0.23 ± 0.05 μmol·kg^{-1} ppm^{-1}) agrees with Ríos et al. (2012) (0.21 ± 0.04 μmol·kg^{-1} ppm^{-1}) and Salt et al., 2015. The uptake of C_{ant} by the AAIW has remained practically constant the last decade. We detect the C_{ant} increase trend in the deepest AABW layer, in line with Ríos et al. (2012) and McNeil et al. (2001), although as expected by their aging, the increase in C_{ant} at the deep layers is more subtle than in subsurface and intermediate waters. The C_{ant} intrusion across all the water column contrasts with the C_{ant} intrusion only into the upper 1000 m depicted by the eMLR method (Salt et al., 2015). The increase of C_{ant} in AABW was not detected under the eMLR approach (Salt et al., 2015) because it is based on repeated sections 1994–2011 not separated in time more than two decades (Ríos et al., 2012). The existence of the transient tracer CFC-12 in deep layers of the South Atlantic (Tanhua et al., 2017) agrees with the idea that C_{ant} concentrations should be present. Although the anthropogenic influence has reached the deepest layers, the small magnitude of their signals is not enough from a chemical perspective to infer significant changes in $_{xc}[CO_3^{2-}]$ (Fig. 5) or other carbon variables (pH, DIC, CO_3, $\Omega_{aragonite}$, Supp. Info Fig. S3).

The $_{xc}[CO_3^{2-}]$ of deep waters are lower than those found in the deep waters of the Northeast Atlantic (Fontela et al., 2020). Ocean acidification decreases the $_{xc}[CO_3^{2-}]$, that is, the amount of carbonate available for marine calcifiers. Here we show that it is extremely likely that the anthropogenic perturbation in the ocean carbon cycle is decreasing the concentration of $_{xc}[CO_3^{2-}]$ in the upper and intermediate layers. The classical pattern of surface waters showing higher acidification trends than subsurface waters and intermediate waters due direct atmospheric uptake is altered in the Argentine Basin. Here, SAMW has a rate of $_{xc}[CO_3^{2-}]$ loss that is higher (-0.47 ± 0.05 μmol·kg^{-1} ppm^{-1}) than the waters above it (SACW, -0.39 ± 0.04 μmol·kg^{-1} ppm^{-1}). The same pattern of water mass acidification is also seen in pH: SAMW has a rate of pH decrease of $-1.50 \pm 0.09 \times 10^{-3}$ pH units ppm^{-1} while for the SACW is $-1.06 \pm 0.1 \times 10^{-3}$ pH units ppm^{-1} (Table 2). Recalling that C_{ant} uptake is larger in SACW (Table 2, Fig. 4), this means that modal and intermediate waters are intrinsically more sensitive to variations in their total carbon content. The low buffering capacity of SAMW and AAIW (Salt et al., 2015; González-Dávila et al., 2011) implies larger acidification for the same C_{ant} input that in SACW. When expressed with respect to the time in years the rate of pH decrease in SAMW (AAIW) has been reported as $-1.8 \sim -1.4 \times 10^{-3}$ pH units·yr^{-1} ($-1.4 \sim -1.2 \times 10^{-3}$ pH units·yr^{-1}) (Ríos et al., 2015; Salt et al., 2015). In the Argentine Basin, for the period 1972–2019, the pH decrease in SAMW and AAIW is almost twice that values (Supp. Info Table S3): -2.8×10^{-3} pH units·yr^{-1} and -2.2×10^{-3} pH units·yr^{-1}, respectively. We suggest that current acidification trends in modal and intermediate waters are the combined result of the anthropogenic acidification signal reinforced by natural processes (Ríos et al., 2015). The relative influence of anthropogenic versus natural processes can be visualized comparing the theoretical decrease in pH computed with the C_{ant} rate against the observed pH rate of decrease (Table 2). The fraction of change not explained by the C_{ant} uptake is the influence of DIC_{nat} in the pH decrease. The increase in DIC_{nat} explains the 27% of the pH decrease in SACW and the 44% in SAMW. In AAIW the increase in DIC_{nat} is responsible for the 40% of the observed pH decrease. The large rate of acidification in modal and intermediate waters is boosted by organic matter remineralization and the consequent oxygen decrease (increase in apparent oxygen utilization (AOU), Supp. Info Fig. S5). In AAIW, the observed trends for DIC_{nat}, AOU and O_2 supports that the natural fraction of acidification is likely related with an increase in biological remineralization. The deoxygenation trend is in line with the significant oxygen loss in the South Atlantic since 1960 (Schmidtko et al., 2017). Furthermore, (i) buffering capacities are progressively lost with the uptake of C_{ant} (González-Dávila et al., 2011); (ii) the uptake of CO_2^{atm} by the ocean in general (Landschützer et al., 2016), and the Argentine Basin specifically (Rödenbeck et al., 2015), is increasing since the onset of the XXIst century; and (iii) the growth rate of CO_2^{atm} has also increased during the last decade (Dlugokencky and Tans, 2020) where the previous studies (Ríos et al., 2012; Salt et al., 2015) does not have measurements. The combined action of these processes with the downwelling of recently formed water masses (Jullion et al., 2010) made the Argentine Basin a hotspot to detect chemical changes in South Atlantic water masses.

It has been reported that AAIW will become undersaturated at the end of the XXIst century (Salt et al., 2015). In the Argentine Basin, if the rate of $_{xc}[CO_3^{2-}]$ decrease is maintained, AAIW will become undersaturated in two decades, anticipating the previous prediction in sixty years. Under a business-as-usual scenario (Shared Socioeconomical Pathway SSP 5.85, Riahi et al., 2017), with the current trend of CO_2^{atm} increase and $_{xc}[CO_3^{2-}]$ lose SAMW will be also in undersaturation at the end of the century. The running out of $_{xc}[CO_3^{2-}]$ from the surface to mid-layers will suppose a decrease in the volume of suitable habitat for aragonitic organisms (Negrete-García et al., 2019).

5. Conclusion

Anthropogenic CO_2 and ocean acidification in Argentine Basin water masses have been evaluated with an assembled database of carbon measurements from eleven oceanographic cruises that spans the time period 1972–2019. In that 47 years, the mean annual concentration of CO_2^{atm} in the Southern Hemisphere increased in 83 ppm (from 325 to 408 ppm), altering the chemical signatures of Argentine Basin water masses at the time of its formation. Anthropogenic CO_2^{atm} uptaken by the ocean (C_{ant}) has provoked ocean acidification and a significant decrease in the amount of carbonate available for aragonitic organisms in the water masses SACW, SAMW and AAIW. In the last five decades there was a fast acidification in SAMW and AAIW with rates of pH decrease larger than 2 thousandths pH units·yr^{-1}. Besides C_{ant} uptake, these acidification trends in modal and intermediate waters are boosted by natural processes. Since Argentine Basin is a zone of subduction where the anthropogenic influence is fast conveyed below subtropical waters, the uptake of C_{ant} affects all depth levels, including the deepest AABW. With the inertia of the CO_2^{atm} concentration system, even if carbon emissions ceased right now, the progression towards undersaturation of AAIW in the Argentine Basin will be unavoidable.

Credit authorship contribution statement

M.F. and F.F.P. wrote the manuscript. M.F. and F.F.P. analyzed the data. M.F. prepared all the figures. M.F., F.F.P., A.V. and M.G. have contributed to the acquisition of data, have participated in the results discussion and have reviewed the manuscript and supporting information.

Declaration of competing interest

The authors declare that they have no known competing financial interests or personal relationships that could have appeared to influence the work reported in this paper.

Acknowledgements

For this work M. Fontela was funded by Portuguese national funds from FCT - Foundation for Science and Technology through project UIDB/Multi/04326/2020 and CEECINST/00114/2018. A. Velo and F. F. Pérez were supported by the BOCATS2 Project (PID2019-104279GB-C21) co-funded by the Spanish Government and the Fondo Europeo de Desarrollo Regional (FEDER). A. Velo, M.Gilcoto and F. F. Pérez were supported by the European Union's Horizon 2020 research and innovation program under grant agreement No 820989 (project COMFORT,

Our common future ocean in the Earth system-quantifying coupled cycles of carbon, oxygen and nutrients for determining and achieving safe operating spaces with respect to tipping points). The work reflects only the author's/authors' view; the European Commission and their executive agency are not responsible for any use that may be made of the information the work contains. The authors are grateful to the crew, technicians and scientists that contributed to data acquisition in these oceanographic cruises. The authors are grateful to the Global Ocean Data Analysis Project (GLODAP, www.glodap.info) data product that provides access to quality controlled biogeochemical data.

Appendix A. Supplementary data

Supplementary data to this article can be found online at https://doi.org/10.1016/j.scitotenv.2021.146570.

References

Álvarez, M., Brea, S., Mercier, H., Álvarez-Salgado, X.A., 2014. Mineralization of biogenic materials in the water masses of the South Atlantic Ocean. I: Assessment and results of an optimum multiparameter analysis. Prog. Oceanogr. https://doi.org/10.1016/j.pocean.2013.12.007.

Anilkumar, N., Chacko, R., Sabu, P., George, J.V., 2015. Freshening of Antarctic bottom water in the Indian Ocean sector of Southern Ocean. Deep. Res. Part II Top. Stud. Oceanogr. https://doi.org/10.1016/j.dsr2.2015.03.009.

Artana, C., Ferrari, R., Koenig, Z., Sennéchael, N., Saraceno, M., Piola, A.R., Provost, C., 2018. Malvinas current volume transport at 41°S: A 24 yearlong time series consistent with mooring data from 3 decades and satellite altimetry. J. Geophys. Res. Ocean. https://doi.org/10.1002/2017JC013600.

Behrenfeld, M.J., Falkowski, P.G., 1997. Photosynthetic rates derived from satellite-based chlorophyll concentration. Limnol. Oceanogr. https://doi.org/10.4319/lo.1997.42.1.0001.

Bengtsson, H., 2018. R. MATLAB: read and write MAT files and call MATLAB from within R.

Caldeira, K., Wickett, M.E., 2003. Anthropogenic carbon and ocean pH. Nature 425, 365. https://doi.org/10.1038/425365a.

Ciais, P., Tan, J., Wang, X., Roedenbeck, C., Chevallier, F., Piao, S.L., Moriarty, R., Broquet, G., Le Quéré, C., Canadell, J.G., Peng, S., Poulter, B., Liu, Z., Tans, P., 2019. Five decades of northern land carbon uptake revealed by the interhemispheric CO2 gradient. Nature. https://doi.org/10.1038/s41586-019-1078-6.

De Lavergne, C., Palter, J.B., Galbraith, E.D., Bernardello, R., Marinov, I., 2014. Cessation of deep convection in the open Southern Ocean under anthropogenic climate change. Nat. Clim. Chang. https://doi.org/10.1038/nclimate2132.

Dickson, A.G., 1990. Standard potential of the reaction: AgCl(s) + 1 2H2(g) = Ag (s) + HCl(aq), and and the standard acidity constant of the ion HSO4- in synthetic sea water from 273.15 to 318.15 K. J. Chem. Thermodyn. https://doi.org/10.1016/0021-9614(90)90074-Z.

Dickson, A.G., Sabine, C.L., Christian, J.R., 2007. Guide to Best Practice for Ocean CO2 Measurements. PICES Spec. Publ.

Dlugokencky, E., Tans, P., 2020. Trends in Atmospheric Carbon Dioxide [WWW Document]. Natl. Ocean. Atmos. Adm. Earth Syst. Res. Lab.

Dragulescu, A., Arendt, C., 2020. xlsx: Read, Write, Format Excel 2007 and Excel 97/2000/XP/2003 Files.

Evans, G.R., McDonagh, E.L., King, B.A., Bryden, H.L., Bakker, D.C.E., Brown, P.J., Schuster, U., Speer, K.G., van Heuven, S.M.A.C., 2017. South Atlantic interbasin exchanges of mass, heat, salt and anthropogenic carbon. Prog. Oceanogr. 151, 62–82. https://doi.org/10.1016/j.pocean.2016.11.005.

Feely, R.A., Byrne, R.H., Betzer, P.R., Gendron, J.F., Acker, J.G., 1984. Factors influencing the degree of saturation of the surface and intermediate waters of the North Pacific ocean with respect to aragonite. J. Geophys. Res. 89, 631–640. https://doi.org/10.1029/jc089ic06p10631.

Fontela, M., 2021. mfontela/ArgentineBasin: Tracer trends in Argentine Basin Water Masses. Zenodo. (Version v1.0) https://zenodo.org/record/4589961. doi:https://doi.org/10.5281/ZENODO.4589961.

Fontela, M., Mercier, H., Pérez, F.F., 2019. Long-term integrated biogeochemical budget driven by circulation in the eastern subpolar North Atlantic. Prog. Oceanogr. 173, 51–65. https://doi.org/10.1016/j.pocean.2019.02.004.

Fontela, M., Pérez, F.F., Carracedo, L.I., Padín, X.A., Velo, A., García-Ibañez, M.I., Lherminier, P., 2020. The Northeast Atlantic is running out of excess carbonate in the horizon of cold-water corals communities. Sci. Rep. 10. https://doi.org/10.1038/s41598-020-71793-2.

Fröb, F., Olsen, A., Pérez, F.F., Garciá-Ibáñez, M.I., Jeansson, E., Omar, A., Lauvset, S.K., 2018. Inorganic carbon and water masses in the Irminger Sea since 1991. Biogeosciences. https://doi.org/10.5194/bg-15-51-2018.

Gattuso, J.-P., Epitalon, J.-M., Lavigne, H., Orr, J., 2020. Seacarb: seawater carbonate chemistry. https://cran.r-project.org/package=seacarb.

González-Dávila, M., Santana-Casiano, J.M., Fine, R.A., Happell, J., Delille, B., Speich, S., 2011. Carbonate system in the water masses of the Southeast Atlantic sector of the Southern Ocean during February and march 2008. Biogeosciences. https://doi.org/10.5194/bg-8-1401-2011.

Gruber, N., Clement, D., Carter, B.R., Feely, R.A., van Heuven, S., Hoppema, M., Ishii, M., Key, R.M., Kozyr, A., Lauvset, S.K., Lo Monaco, C., Mathis, J.T., Murata, A., Olsen, A., Perez, F.F., Sabine, C.L., Tanhua, T., Wanninkhof, R., 2019. The oceanic sink for anthropogenic CO2 from 1994 to 2007. Science 80 (363), 1193–1199. https://doi.org/10.1126/science.aau5153.

Jiang, L.Q., Feely, R.A., Carter, B.R., Greeley, D.J., Gledhill, D.K., Arzayus, K.M., 2015. Climatological distribution of aragonite saturation state in the global oceans. Glob. Biogeochem. Cycles https://doi.org/10.1002/2015GB005198.

Johnson, G.C., Cadot, C., Lyman, J.M., McTaggart, K.E., Steffen, E.L., 2020. Antarctic bottom water warming in the Brazil Basin: 1990s through 2020, from WOCE to Deep Argo. Geophys. Res. Lett. https://doi.org/10.1029/2020GL089191.

Jullion, L., Heywood, K.J., Naveira Garabato, A.C., Stevens, D.P., 2010. Circulation and water mass modification in the Brazil-Malvinas confluence. J. Phys. Oceanogr. https://doi.org/10.1175/2009JPO4174.1.

Jullion, L., Garabato, A.C.N., Meredith, M.P., Holland, P.R., Courtois, P., King, B.A., 2013. Decadal freshening of the antarctic bottom water exported from the weddell sea. J. Clim. https://doi.org/10.1175/JCLI-D-12-00765.1.

Key, R.M., Tanhua, T., Olsen, A., Hoppema, M., Jutterström, S., Schirnick, C., Van Heuven, S., Kozyr, A., Lin, X., Velo, A., Wallace, D.W.R., Mintrop, L., 2010. The CARINA data synthesis project: introduction and overview. Earth Syst. Sci. Data. https://doi.org/10.5194/essd-2-105-2010.

Key, R.M., Olsen, A., van Heuven, S., Lauvset, S.K., Velo, A., Lin, X., Schirnick, C., Kozyr, A., Tanhua, T., Hoppema, M., Jutterström, S., Steinfeldt, R., Jeansson, E., Ishi, M., Perez, F.F., Suzuki, T., 2015. Global Ocean Data Analysis Project, Version 2 (GLODAPv2), ORNL/CDIAC-162, ND-P093. Carbon Dioxide Information Analysis Center, Oak Ridge National Laboratory. US Department of Energy, Oak Ridge, Tennessee https://doi.org/10.3334/CDIAC/OTG.NDP093_GLODAPv2.

Khatiwala, S., Tanhua, T., Mikaloff Fletcher, S., Gerber, M., Doney, S.C., Graven, H.D., Gruber, N., McKinley, G.A., Murata, A., Ríos, A.F., Sabine, C.L., 2013. Global Ocean storage of anthropogenic carbon. Biogeosciences 10, 2169–2191. https://doi.org/10.5194/bg-10-2169-2013.

Landschützer, P., Gruber, N., Bakker, D.C.E., 2016. Decadal variations and trends of the global ocean carbon sink. Glob. Biogeochem. Cycles https://doi.org/10.1002/2015GB005359.

Lo Monaco, C., Metzl, N., Poisson, A., Brunet, C., Schauer, B., 2005. Anthropogenic CO2 in the Southern Ocean: distribution and inventory at the Indian-Atlantic boundary (World Ocean Circulation Experiment line I6). J. Geophys. Res. Ocean. 110. https://doi.org/10.1029/2004JC002643.

Lueker, T.J., Dickson, A.G., Keeling, C.D., 2000. Ocean pCO2 calculated from dissolved inorganic carbon, alkalinity, and equations for K1 and K2: validation based on laboratory measurements of CO2 in gas and seawater at equilibrium. Mar. Chem. https://doi.org/10.1016/S0304-4203(00)00022-0.

McCartney, M., 1982. The subtropical recirculation of mode waters. J. Mar. Res. 40, 427–464.

McNeil, B.I., Tilbrook, B., Matear, R.J., 2001. Accumulation and uptake of anthropogenic CO2 in the Southern Ocean, south of Australia between 1968 and 1996. J. Geophys. Res. Ocean. https://doi.org/10.1029/2000jc000331.

McNeil, B.I., Metzl, N., Key, R.M., Matear, R.J., Corbiere, A., 2007. An empirical estimate of the Southern Ocean air-sea CO2 flux. Glob. Biogeochem. Cycles https://doi.org/10.1029/2007GB002991.

Meinen, C.S., Perez, R.C., Dong, S., Piola, A.R., Campos, E., 2020. Observed Ocean bottom temperature variability at four sites in the northwestern argentine basin: evidence of decadal deep/abyssal warming amidst hourly to interannual variability during 2009–2019. Geophys. Res. Lett. https://doi.org/10.1029/2020GL089093.

Mémery, L., Arhan, M., Alvarez-Salgado, X.A., Messias, M.J., Mercier, H., Castro, C.G., Rios, A.F., 2000. The water masses along the western boundary of the south and equatorial Atlantic. Prog. Oceanogr. https://doi.org/10.1016/S0079-6611(00)00032-X.

Menezes, V.V., Macdonald, A.M., Schatzman, C., 2017. Accelerated freshening of Antarctic bottom water over the last decade in the southern Indian Ocean. Sci. Adv. https://doi.org/10.1126/sciadv.1601426.

Mikaloff Fletcher, S.E., Gruber, N., Jacobson, A.R., Doney, S.C., Dutkiewicz, S., Gerber, M., Follows, M., Joos, F., Lindsay, K., Menemenlis, D., Mouchet, A., Müller, S.A., Sarmiento, J.L., 2006. Inverse estimates of anthropogenic CO2 uptake, transport, and storage by the ocean. Glob. Biogeochem. Cycles https://doi.org/10.1029/2005GB002530.

Millero, F.J., Feistel, R., Wright, D.G., McDougall, T.J., 2008. The composition of standard seawater and the definition of the reference-composition salinity scale. Deep. Res. Part I Oceanogr. Res. Pap. https://doi.org/10.1016/j.dsr.2007.10.001.

Negrete-García, G., Lovenduski, N.S., Hauri, C., Krumhardt, K.M., Lauvset, S.K., 2019. Sudden emergence of a shallow aragonite saturation horizon in the Southern Ocean. Nat. Clim. Chang. https://doi.org/10.1038/s41558-019-0418-8.

Olsen, A., Key, R.M., Van Heuven, S., Lauvset, S.K., Velo, A., Lin, X., Schirnick, C., Kozyr, A., Tanhua, T., Hoppema, M., Jutterström, S., Steinfeldt, R., Jeansson, E., Ishii, M., Pérez, F.F., Suzuki, T., 2016. The global ocean data analysis project version 2 (GLODAPv2) - an internally consistent data product for the world ocean. Earth Syst. Sci. Data. https://doi.org/10.5194/essd-8-297-2016.

Olsen, A., Lange, N., Key, R.M., Tanhua, T., Álvarez, M., Becker, S., Bittig, H.C., Carter, B.R., Cotrim da Cunha, L., Feely, R.A., van Heuven, S., Hoppema, M., Ishii, M., Jeansson, E., Jones, S.D., Jutterström, S., Karlsen, M.K., Kozyr, A., Lauvset, S.K., Lo Monaco, C., Murata, A., Pérez, F.F., Pfeil, B., Schirnick, C., Steinfeldt, R., Suzuki, T., Telszewski, M., Tilbrook, B., Velo, A., Wanninkhof, R., 2019. GLODAPv2.2019 – an update of GLODAPv2. Earth Syst. Sci. Data 11, 1437–1461. https://doi.org/10.5194/essd-11-1437-2019.

Olsen, A., Lange, N., Key, R.M., Tanhua, T., Bittig, H.C., Kozyr, A., Álvarez, M., Azetsu-Scott, K., Becker, S., Brown, P.J., Carter, B.R., Cotrim Da Cunha, L., Feely, R.A., Van Heuven, S., Hoppema, M., Ishii, M., Jeansson, E., Jutterström, S., Landa, C.S., Lauvset, S.K., Michaelis, P., Murata, A., Pérez, F.F., Pfeil, B., Schirnick, C., Steinfeldt, R., Suzuki, T., Tilbrook, B., Velo, A., Wanninkhof, R., Woosley, R.J., 2020. An updated version of the

global interior ocean biogeochemical data product, GLODAPv2.2020. Earth Syst. Sci. Data. https://doi.org/10.5194/essd-12-3653-2020.
Orr, J.C., Fabry, V.J., Aumont, O., Bopp, L., Doney, S.C., Feely, R.A., Gnanadesikan, A., Gruber, N., Ishida, A., Joos, F., Key, R.M., Lindsay, K., Maier-Reimer, E., Matear, R., Monfray, P., Mouchet, A., Najjar, R.G., Plattner, G.K., Rodgers, K.B., Sabine, C.L., Sarmiento, J.L., Schlitzer, R., Slater, R.D., Totterdell, I.J., Weirig, M.F., Yamanaka, Y., Yool, A., 2005. Anthropogenic Ocean acidification over the twenty-first century and its impact on calcifying organisms. Nature 437, 681–686. https://doi.org/10.1038/nature04095.
Orr, J.C., Epitalon, J.M., Dickson, A.G., Gattuso, J.P., 2018. Routine uncertainty propagation for the marine carbon dioxide system. Mar. Chem. https://doi.org/10.1016/j.marchem.2018.10.006.
Orselli, I.B.M., Kerr, R., Ito, R.G., Tavano, V.M., Mendes, C.R.B., Garcia, C.A.E., 2018. How fast is the Patagonian shelf-break acidifying? J. Mar. Syst. https://doi.org/10.1016/j.jmarsys.2017.10.007.
Pante, E., Simon-Bouhet, B., 2013. Marmap: A package for importing, plotting and analyzing bathymetric and topographic data in R. PLoS One https://doi.org/10.1371/journal.pone.0073051.
Pardo, P.C., Pérez, F.F., Khatiwala, S., Ríos, A.F., 2014. Anthropogenic CO2 estimates in the Southern Ocean: storage partitioning in the different water masses. Prog. Oceanogr. https://doi.org/10.1016/j.pocean.2013.09.005.
Pérez, F.F., Fraga, F., 1987. Association constant of fluoride and hydrogen ions in seawater. Mar. Chem. https://doi.org/10.1016/0304-4203(87)90036-3.
Pérez, F.F., Vázquez-Rodríguez, M., Louarn, E., Padín, X.A., Mercier, H., Ríos, A.F., 2008. Temporal variability of the anthropogenic CO2 storage in the Irminger Sea. Biogeosciences 5, 1669–1679. https://doi.org/10.5194/bg-5-1669-2008.
Pérez, F.F., Vázquez-Rodríguez, M., Mercier, H., Velo, A., Lherminier, P., Ríos, A.F., 2010. Trends of anthropogenic CO2 storage in North Atlantic water masses. Biogeosciences 7, 1789–1807. https://doi.org/10.5194/bg-7-1789-2010.
Pérez, F.F., Mercier, H., Vázquez-Rodríguez, M., Lherminier, P., Velo, A., Pardo, P.C., Rosón, G., Ríos, A.F., 2013. Atlantic Ocean CO2 uptake reduced by weakening of the meridional overturning circulation. Nat. Geosci. 6, 146–152. https://doi.org/10.1038/ngeo1680.
Perez, F.F., Fontela, M., García-Ibáñez, M.I., Mercier, H., Velo, A., Lherminier, P., Zunino, P., De La Paz, M., Alonso-Pérez, F., Guallart, E.F., Padin, X.A., 2018. Meridional overturning circulation conveys fast acidification to the deep Atlantic Ocean. Nature 554, 515–518. https://doi.org/10.1038/nature25493.
Pörtner, H.O., Roberts, D.C., Masson-Delmotte, V., Zhai, P., Tignor, M., Poloczanska, E., Mintenbeck, K., Nicolai, M., Okem, A., Petzold, J., 2019. IPCC Special Report on the Ocean and Cryosphere in a Changing Climate, IPCC Intergovernmental Panel on Climate Change: Geneva, Switzerland.
Raven, J., Caldeira, K., Elderfield, H., Hoegh-Guldberg, O., Liss, P., Riebesell, U., Shepherd, J., Turley, C., Watson, A., 2005. Ocean acidification due to increasing atmospheric carbon dioxide. R. Soc. 5, 60. https://doi.org/10.1080/02688690801911598.
Ren, K., 2016. rlist: a toolbox for non-tabular data manipulation.
Rhein, M., Kieke, D., Steinfeldt, R., 2015. Advection of North Atlantic Deep Water from the Labrador Sea to the southern hemisphere. J. Geophys. Res. Ocean. 120, 2471–2487. https://doi.org/10.1002/2014JC010605.
Riahi, K., van Vuuren, D.P., Kriegler, E., Edmonds, J., O'Neill, B.C., Fujimori, S., Bauer, N., Calvin, K., Dellink, R., Fricko, O., Lutz, W., Popp, A., Cuaresma, J.C., KC, S., Leimbach, M., Jiang, L., Kram, T., Rao, S., Emmerling, J., Ebi, K., Hasegawa, T., Havlik, P., Humpenöder, F., Da Silva, L.A., Smith, S., Stehfest, E., Bosetti, V., Eom, J., Gernaat, D., Masui, T., Rogelj, J., Strefler, J., Drouet, L., Krey, V., Luderer, G., Harmsen, M., Takahashi, K., Baumstark, L., Doelman, J.C., Kainuma, M., Klimont, Z., Marangoni, G., Lotze-Campen, H., Obersteiner, M., Tabeau, A., Tavoni, M., 2017. The shared socioeconomic pathways and their energy, land use, and greenhouse gas emissions implications: an overview. Glob. Environ. Chang. 42, 153–168. https://doi.org/10.1016/j.gloenvcha.2016.05.009.
Rintoul, S.R., 2007. Rapid freshening of Antarctic bottom water formed in the Indian and Pacific oceans. Geophys. Res. Lett. https://doi.org/10.1029/2006GL028550.
Ríos, A.F., Vázquez-Rodríguez, M., Padin, X.A., Pérez, F.F., 2010. Anthropogenic carbon dioxide in the South Atlantic western basin. J. Mar. Syst. https://doi.org/10.1016/j.jmarsys.2010.06.010.
Ríos, A.F., Velo, A., Pardo, P.C., Hoppema, M., Pérez, F.F., 2012. An update of anthropogenic CO 2 storage rates in the western South Atlantic basin and the role of Antarctic bottom water. J. Mar. Syst. https://doi.org/10.1016/j.jmarsys.2011.11.023.
Ríos, A.F., Resplandy, L., García-Ibáñez, M.I., Fajar, N.M., Velo, A., Padin, X.A., Wanninkhof, R., Steinfeldt, R., Rosón, G., Pérez, F.F., Morel, F.M.M., 2015. Decadal acidification in the water masses of the Atlantic Ocean. Proc. Natl. Acad. Sci. U. S. A. https://doi.org/10.1073/pnas.1504613112.
Rödenbeck, C., Bakker, D.C.E., Gruber, N., Iida, Y., Jacobson, A.R., Jones, S., Landschützer, P., Metzl, N., Nakaoka, S., Olsen, A., Park, G.H., Peylin, P., Rodgers, K.B., Sasse, T.P., Schuster, U., Shutler, J.D., Valsala, V., Wanninkhof, R., Zeng, J., 2015. Data-based estimates of the ocean carbon sink variability - first results of the Surface Ocean pCO2 mapping intercomparison (SOCOM). Biogeosciences. https://doi.org/10.5194/bg-12-7251-2015.
Sabine, C.L., Feely, R.A., Gruber, N., Key, R.M., Lee, K., Bullister, J.L., Wanninkhof, R., Wong, C.S., Wallace, D.W.R., Tilbrook, B., Millero, F.J., Peng, T.H., Kozyr, A., Ono, T., Rios, A.F., 2004. The oceanic sink for anthropogenic CO_2. Science 80. https://doi.org/10.1126/science.1097403.
Salt, L.A., Van Heuven, S.M.A.C., Claus, M.E., Jones, E.M., De Baar, H.J.W., 2015. Rapid acidification of mode and intermediate waters in the southwestern Atlantic Ocean. Biogeosciences. https://doi.org/10.5194/bg-12-1387-2015.
Schlitzer, R., 2020. Ocean Data View, odv.awi.de.
Schmidtko, S., Stramma, L., Visbeck, M., 2017. Decline in global oceanic oxygen content during the past five decades. Nature. https://doi.org/10.1038/nature21399.
Stocker, T.F., Qin, D., Plattner, G.K., Tignor, M.M.B., Allen, S.K., Boschung, J., Nauels, A., Xia, Y., Bex, V., Midgley, P.M., 2013. Climate Change 2013 the Physical Science Basis: Working Group I Contribution to the Fifth Assessment Report of the Intergovernmental Panel on Climate Change, Climate Change 2013 the Physical Science Basis: Working Group I Contribution to the Fifth Assessment Report of the Intergovernmental Panel on Climate Change. https://doi.org/10.1017/CBO9781107415324.
Stramma, L., England, M., 1999. On the water masses and mean circulation of the South Atlantic Ocean. J. Geophys. Res. Ocean. 104, 20863–20883. https://doi.org/10.1029/1999JC900139.
Swift, J.H., Orsi, A.H., 2012. Sixty-four days of hydrography and storms: RVIB Nathaniel B. Palmer's 2011 S04P cruise. Oceanography. https://doi.org/10.5670/oceanog.2012.74.
Talley, L.D., Pickard, G.L., Emery, W.J., Swift, J.H., 2011. Descriptive physical oceanography: an introduction: sixth edition. Descriptive Physical Oceanography: An Introduction: Sixth Edition. https://doi.org/10.1016/C2009-0-24322-4.
Tanhua, T., Hoppema, M., Jones, E.M., Stöven, T., Hauck, J., Dávila, M.G., Santana-Casiano, M., Álvarez, M., Strass, V.H., 2017. Temporal changes in ventilation and the carbonate system in the Atlantic sector of the Southern Ocean. Deep. Res. Part II Top. Stud. Oceanogr. https://doi.org/10.1016/j.dsr2.2016.10.004.
Uppström, L.R., 1974. The boron/chlorinity ratio of deep-sea water from the Pacific Ocean. Deep. Res. Oceanogr. Abstr. https://doi.org/10.1016/0011-7471(74)90074-6.
Valla, D., Piola, A.R., Meinen, C.S., Campos, E., 2018. Strong mixing and recirculation in the northwestern argentine basin. J. Geophys. Res. Ocean. https://doi.org/10.1029/2018JC013907.
Vázquez-Rodríguez, M., Touratier, F., Lo Monaco, C., Waugh, D.W., Padin, X.A., Bellerby, R.G.J., Goyet, C., Metzl, N., Ríos, A.F., Pérez, F.F., 2009. Anthropogenic carbon distributions in the Atlantic Ocean: data-based estimates from the Arctic to the Antarctic. Biogeosciences 6, 439–451. https://doi.org/10.5194/bg-6-439-2009.
Vázquez-Rodríguez, M., Padin, X.A., Pardo, P.C., Ríos, A.F., Pérez, F.F., 2012. The subsurface layer reference to calculate preformed alkalinity and air-sea CO 2 disequilibrium in the Atlantic Ocean. J. Mar. Syst. https://doi.org/10.1016/j.jmarsys.2011.10.008.
Velo, A., Pérez, F.F., Lin, X., Key, R.M., Tanhua, T., De La Paz, M., Olsen, A., Van Heuven, S., Jutterström, S., Ríos, A.F., 2010. CARINA data synthesis project: PH data scale unification and cruise adjustments. Earth Syst. Sci. Data. https://doi.org/10.5194/essd-2-133-2010.
Venables, W.N., Ripley, B.D., 2002. Modern Applied Statistics with S Fourth Edition by, World.
Wanninkhof, R., Doney, S.C., Bullister, J.L., Levine, N.M., Warner, M., Gruber, N., 2010. Detecting anthropogenic CO_2 changes in the interior Atlantic Ocean between 1989 and 2005. J. Geophys. Res. Ocean. https://doi.org/10.1029/2010JC006251.
Wickham, H., Averick, M., Bryan, J., Chang, W., McGowan, L., François, R., Grolemund, G., Hayes, A., Henry, L., Hester, J., Kuhn, M., Pedersen, T., Miller, E., Bache, S., Müller, K., Ooms, J., Robinson, D., Seidel, D., Spinu, V., Takahashi, K., Vaughan, D., Wilke, C., Woo, K., Yutani, H., 2019. Welcome to the Tidyverse. J. Open Source Softw. https://doi.org/10.21105/joss.01686.
Zenk, W., Morozov, E., 2007. Decadal warming of the coldest Antarctic bottom water flow through the Vema Channel. Geophys. Res. Lett. https://doi.org/10.1029/2007GL030340.